Astronomy & Astrophysics manuscript no. Template_AA
September 1, 2019

Binary black holes in AGN accretion disks: merger time scales and gravitational wave rate density estimates

MG[1,2], MH(?)[2], WI[2,3], PJ(?)[2], and ST[2]

[1] Institute of Physics, ETH Zürich, Zürich, Switzerland.
[2] Physik-Institut, Universität Zürich, Zürich, Switzerland
[3] Institute of Astronomy, Madingley Road, Cambridge CB3 0HA
e-mail: xxx@xxx.ch

Received; accepted

ABSTRACT

Context.
Aims.
Methods.
Results.

Key words. Gravitational waves, AGNs, GW rate density

1. Introduction

BBH evolution channels, AGN evolution channel (gaseous disk, EMR counterparts)
Novelity: Analytic model that includes both GW and disk effects on the orbital evolution of binary systems.

2. Binary evolution channel

Binary systems in AGNs give a good source of gravitational waves. However, it is not sufficient to treat the orbital evolution of such embedded binary systems with the purely gravitational wave driven evolution equations alone (include other mechanisms that assists merging, otherwise too long merger times). It is important to understand how the dense gaseous accretion disk of the AGN affects the evolution of binary black holes, as this will have an influence on the merger rate of BBHs.

2.1. Gravitational wave emission

The orbital parameters of a binary system are affected due to the release of gravitational waves. The gravitational wave driven evolution equations of the semi-major axis and the eccentricity for binaries on an elliptic Keplerian orbit read (Peters & Mathews (1963))

$$\dot{a}_{\rm GW} = -\frac{64}{5}\frac{G^3}{c^5}\frac{\mu M^2}{a^3}\frac{1}{(1-e^2)^{7/2}}\left(1+\frac{73}{24}e^2+\frac{37}{96}e^4\right), \quad (1)$$

and

$$\dot{e}_{\rm GW} = -\frac{304}{15}\frac{G^3}{c^5}\frac{\mu M^2}{a^4}\frac{e}{(1-e^2)^{5/2}}\left(1+\frac{121}{304}e^2\right). \quad (2)$$

2.2. Disk-binary interaction

Numerical simulations suggest the building and presence of a depleted cavity inside of which the binary resides. The gas orbiting around this cavity is referred to as the circumbinary accretion disk (CBD). The evolution of the semi-major axis and of the orbital eccentricity are driven by tidal and viscous interactions between the binary and the CBD. We will set up a simplified and idealized model of this picture. We will see that the here detailed disk interaction facilitates the merging of the binary system.

From now on, let us assume that the binary system has quickly excavated an inner cavity in the gas distribution and that the central cavity is surrounded by a circumbinary accretion disk. Unfortunately, we don't know the timescale for formation of the cavity, because usually also the simulations already assume an initial cavity. For simplicity we also assume that neither the primary nor the secondary mass have their own minidisks. We aim to relate the viscous angular momentum flux in the inner region of the circumbinary disk to the orbital evolution of the binary.

Numerical simulations (see *e.g.* Lubow & Artymowicz Lubow (1996)) suggest that the size of the central cavity extends to about twice the semi-major axis of the binary orbit (as seen from the center of mass frame). This holds for binaries on circular orbits. Artymowicz & Lubow Artymowicz & Lubow (1994) showed through simulations that with increasing eccentricity the location of the inner edge progresses outwards, in their simulations from $r_{\rm in} \approx 1.9a$ for $e \approx 0.02$ to $r_{\rm in} \approx 3a$ for $e \approx 0.6$. These findings are also in accordance with simulations performed by Hayasaki *et al.* Hayasaki et al. (2007) where for $e = 0.5$ the inner edge was located at $r_{\rm in} \approx 2.8a$. Also, the above simulations suggest that the gap size seems to be approximately the same for different binary mass ratios q. Inspired by their findings, we thus estimate the inner edge of the circumbinary disk to be set by the twice the distance of the binary at apocenter, *i.e.* $r_{\rm in} = 2a(1+e)$, and extrapolate this estimate also to eccentricities up to unity. This is not justified and it is likely that modifications occur for

higher eccentricities. Towards more definite answers, one has to admit, there is no way around of performing hydrodynamical simulations. The simulations also show that the cavity is shaped circularly, independent of the eccentricity of the binary orbit.

Tidal torques from the binary are expected to act significantly only on a narrow annulus at the inner edge of the CBD and are thus assumed to be zero outside of some cutoff radius r_Λ, which is very similar to $r_{\rm in}$. Thus the effect of the binary torque on the disk evolution can be accounted for via equation (**??**) by imposing suitable boundary conditions at the inner edge of the disk. From the previous subsection we deduce

$$\left(\frac{\partial(\Omega_{\rm CBD}r^2)}{\partial r}\right)\dot{M} = \frac{\partial(T_{\rm visc})}{\partial r} + \left(\frac{\partial(\Omega_{\rm CBD}r^2)}{\partial r}\right)\frac{4\pi\Sigma_g\tilde{T}_{\rm ext}}{\Omega_{\rm CBD}}. \quad (3)$$

Integrating from r_b to r_Λ we obtain

$$T_{\rm visc}(r_\Lambda) = -8\pi\int_{r_b}^{r_\Lambda} dr\, r\Sigma_g\tilde{T}_{\rm ext} + 2\int_{r_b}^{r_\Lambda} dr\, r\Omega_{\rm CBD}\dot{M}; \quad (4)$$

we have set $T_{\rm visc}(r_b) = 0$ because of the clean gap assumption.

The first integral on the right hand side is the total torque the binary exerts on the disk, that is to say, the rate of the angular momentum injection into the disk by the binary. As long as the evolution of the binary is driven predominantly by the interaction with the disk, conservation of angular momentum guarantees that this term equals the change of angular momentum of the binary. In the right integral on the right side we can write

$$|\dot{M}| = 3\pi\Sigma_g\nu = 3\pi\Sigma_g\alpha c_s^2/\Omega_{\rm CBD}. \quad (5)$$

Because of the clean gap assumption, the disk surface density Σ_g is zero for $r < r_{in}$. Thus we approximate the integral by

$$\begin{aligned}\Delta &\equiv 6\pi\alpha c_s^2\Sigma_g(r_{in})\int_{r_{in}}^{r_\Lambda} dr\, r\\ &= 3\pi\alpha c_s^2\Sigma_g(r_{in})\left[r_\Lambda^2 - r_{in}^2\right]\\ &\approx 3\pi\alpha c_s^2\Sigma_g(r_{in})\delta r_{in},\end{aligned}$$

where we set the disk density in the small radial annulus $[r_{\rm in}, r_\Lambda]$ around the cavity edge to $\Sigma_g(r_{in})$ since $r_\Lambda - r_{\rm in} = \delta/2 \ll r_{\rm in}$ and since we have no model to resolve the surface density of the CBD down to this scale.

From here forward, we will work in the reference frame of the binary system. The binary injects angular momentum into the disk, so we require $\dot{L}_b < 0$. According to this convention, in the binary reference frame the sign of the viscous torque must be opposite to that of equation (**??**). Thus the viscous torque reads $T_{\rm visc}(2a(1+e)) = 12\pi\alpha c_s^2\Sigma_g a^2(1+e)^2$. Here c_s and Σ_g are to be evaluated at $r_{\rm in}$ (however, towards the end of this section we will have abandoned the hope to actually model the profile of the CBD). As $T_{\rm visc}(2a(1+e))$ is a few order of magnitudes higher than Δ, we neglect Δ henceforth. In the binary frame, equation (4) therefore translates into

$$T_{\rm visc}(r_{\rm in}) = -\dot{L}_b. \quad (6)$$

We impose a further assumption to the particular evolution model, namely that the binary-disk interaction may well be approximated as an adiabatic process. In other words, we assume that the timescale of the disk-binary interaction is much larger than some characteristic timescale of the binary, like its orbital period. This assumption is supported by the simulations because they show the maintenance of the circular shape of the cavity across a large spectrum of eccentricities. Phrased in another way, as the hydrodynamical simulations do not show signs of non-circular cavity shapes even for large eccentricities, we assume the torque to act on average axially-symmetrically onto the disk. This is an idealised assumption and for a deeper understanding one needs a microscopic understanding of the disk-binary interaction that does not rely on a macroscopic orbital averaging of dynamical parameters. Under the adiabatic assumption, the change in the binary energy can be related to its change in angular momentum through the orbital frequency,

$$\dot{E}_b = \Omega\dot{L}_b. \quad (7)$$

Note that $\dot{L}_b < 0$, so $\dot{E}_b < 0$ and therefore the binary system always evolves toward lower energy. In particular an initially bound orbit always stays on an elliptic orbit. Energy conservation implies that energy is deposited in the circumbinary disk and this dissipated energy may *e.g.* heat up the disk material. From the evolution equation (**??**) for the semi-major axis of the binary orbit and the binary energy $E_b = -\frac{\Omega L_b}{2\sqrt{1-e^2}}$ it follows that

$$\frac{\dot{a}}{a} = -\frac{\dot{E}_b}{E_b} = -\frac{T_{\rm visc}(r_{\rm in})}{L_b}2\sqrt{1-e^2} \quad (8)$$

$$= -2\frac{T_{\rm visc}(r_{\rm in})}{\mu\Omega a^2}, \quad (9)$$

where the last equation follows by substituting the orbital angular momentum (**??**). Substituting the explicit formula for the viscous torque results in

$$\dot{a} = -\frac{24\pi a\alpha c_s^2\Sigma_g(1+e)^2}{\mu\Omega}. \quad (10)$$

Starting from the standard evolution equation (**??**), we similarly get for the evolution of the eccentricity the expression

$$\dot{e} = \frac{1-e^2}{e}\left(\frac{1}{\sqrt{1-e^2}} - 1\right)\frac{T_{\rm visc}(r_{\rm in})}{\mu\Omega a^2} \quad (11)$$

$$= \frac{(1+e)^2}{e}(\sqrt{1-e^2} + e^2 - 1)\frac{12\pi\alpha c_s^2\Sigma_g}{\mu\Omega}. \quad (12)$$

Inspection of the evolution equations shows that in this model for $a \neq 0$ the semi-major axis decreases in time and the orbital eccentricity increases in time. Even though we have $\dot{e} \geq 0$, the orbit cannot become unbound since the orbit's energy is decreasing. In effect, the disk-binary dynamics will drive the binary into a regime where gravitational wave emissions will dominate the orbital evolution.

We can divide equation (10) by equation (12) and solve the resulting differential equation. We get

$$a(e) = a_0\left(\frac{1-\sqrt{1-e_0^2}}{1-\sqrt{1-e^2}}\right)^2, \quad (13)$$

with initial semi-major axis a_0 and initial eccentricity e_0. But as indicated above, it would not be meaningful to assert that the disk dynamics alone can provide a full description of the orbital evolution. In fact, a binary evolution premised purely on (10) and (12) seems unphysical, for $e \to 1$ and $a \to 0$ indicates that the orbit enters a regime where gravitational wave emission

cannot be neglected.

In chapter (**??**) we need to insert values for α, Σ_g, c_s and h/r of the CBD. We set those quantities of the circumbinary disk equal to those of the background disk at the location where the binary resides within the background disk. One may argue that the quantities taken at the inner edge of the CBD should not differ significantly from the quantities taken at the outer edge of the CBD and there those quantities should not differ from their values in the background disk. The inspiration for using this assumption comes from Baruteau *et al.* Baruteau et al. (2010), who use this assumption for a similar problem. We realize that this assumption is not satisfactory, but due to the lack of a better alternative we will use it.

3. Analysis of evolution channel

Both gravitational wave emission and the disk interaction affect the evolution of the binary system. To investigate the dynamics of the interplay between both effects, we combine $\dot{a}_{\text{disk-binary}}$ (expression (10)) and $\dot{e}_{\text{disk-binary}}$ (expression (12)) of the disk-driven orbital evolution channel with the corresponding gravitational wave driven evolution equations $\dot{a}_{\text{GW}}$ and $\dot{e}_{\text{GW}}$ of section (**??**). The combined dynamics is thus described by the evolution equations

$$\begin{aligned} \dot{a} &= \dot{a}_{\text{GW}} + \dot{a}_{\text{disk-binary}}, \\ \dot{e} &= \dot{e}_{\text{GW}} + \dot{e}_{\text{disk-binary}}. \end{aligned} \tag{14}$$

We integrate this coupled system of differential equations numerically. The numerical integration yields the temporal evolution of the semi-major axis and the eccentricity that results from the evolution channel dictated by the coupled evolution equations (14). Of particular interest is the time to merger of a binary system with orbital parameters M and μ, initial conditions a_0 and e_0 and that is embedded in a CBD with disk parameters Σ, c_s, α and aspect ratio h/r (recall from the previous subsection the assumption that relates those quantities to the corresponding ones of the background disk). The merger time is taken as the abscissa where the numerical solution $a(t)$, or equivalently $e(t)$, approaches the abscissa axis.

At most values of the semi-major axis a the disk-binary interaction dominates the gravitational wave emission. Only at the latest stages of inspiral when a is sufficiently low, gravitational emission becomes important. The combined evolution reduces the purely gravitational wave-driven merger time by several orders of magnitudes. Binary systems with a certain configuration of orbital parameters that are not embedded into a disk would not merge within a Hubble time, which is about 1.4×10^{10} years. A gaseous environment would provide a mechanism for such binaries to merge. Let us illustrate the above assertions by a numerical example. Figure (1) shows, as a function of the orbit's initial eccentricity, the purely gravitational wave-driven merger times (blue) and those where in addition disk interactions are taken into account (green). For the disk parameters we used $M_{\text{SMBH}} = 1 \times 10^7 M_\odot, \alpha = 0.1$, $f_g = 0.1$ and $h/r = 0.01$. The binary's location in the disk is $r = 0.1$ pc and we have set $M = 50 M_\odot$, $\mu = M/4$, $a_0 = 1$ AU. The merger time for $e = 0.01$ premised upon the disk-GW channel is 1.76×10^8 years (compared to 1.01×10^{13} years for the purely GW driven evolution), for $e = 0.99$ it is 1.97×10^5 years (as opposed to 1.69×10^7 years for the purely GW driven evolution). Of course, if the initial semi-major axis a_0 is already sufficiently low, then the orbit evolves due to gravitational radiation alone and the disk interaction has no imprint on the orbital evolution. Using as an illustration the disk parameters of the previous example and an initial eccentricity of $e_0 = 0.3$, then for $a_0 < 0.02$ AU the disk interaction plays no dominant role in the orbital evolution (at $a_0 = 0.02$ AU, the merger time is 1.13×10^6 years).

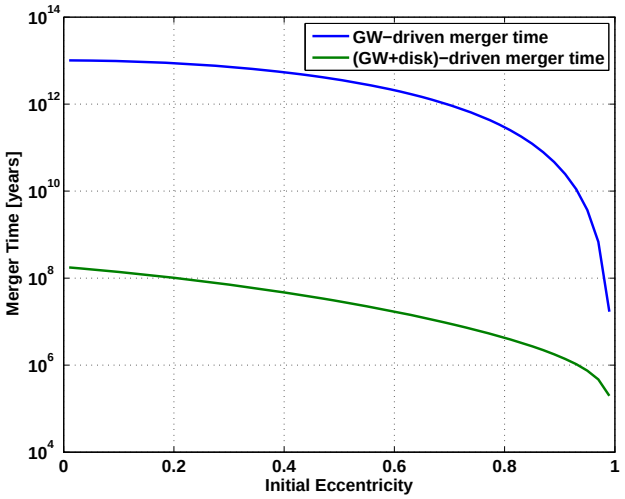

Fig. 1. Merger times as a function of the initial binary eccentricity. The blue curve represents the merger times resulting from GW-driven decay, the green one resulting from both GW emission and disk-binary interaction.

The disk-binary dynamics shrinks the binary's semi-major axis while at the same time it increases the orbit's eccentricity. At a critical semi-major axis, where $\dot{a}_{\text{GW}} = \dot{a}_{\text{disk-binary}}$, the binary evolution changes from being predominately disk driven to being predominately driven by gravitational wave emission. Here is again a numerical illustration. Figure (2) displays the orbit's semi-major axis as a function of the orbit's eccentricity for initial eccentricities e_0 ranging from 0.01 to 0.9. The black circles indicate the transition where $\dot{a}_{\text{GW}}$ starts dominating over $\dot{a}_{\text{disk-binary}}$. The semi-major axis where gravitational wave emission becomes dominating increases as the initial eccentricity increases. However, the higher absolute value of the orbital eccentricity results eventually in a merging that is faster than that for lower initial eccentricities. In the plot, the parameters of the binary are $a_0 = 1$ AU, $M = 50 M_\odot$ and $q = 1$. The binary system is located at $r = 0.1$ pc in a disk with characteristics $M_{\text{SMBH}} = 1 \times 10^7 M_\odot, \alpha = 0.1, f_g = 0.1$ and $h/r = 0.01$. From the figure we also observe that the eccentricity at the transition semi-major axis does not necessarily coincide with the maximum eccentricity reached during the entire orbital evolution. This is because $\dot{a}_{\text{GW}} = \dot{a}_{\text{disk-binary}}$ doesn't necessarily imply $|\dot{e}_{\text{GW}}| = |\dot{e}_{\text{disk-binary}}|$.

In figure (3) we plot the orbital decay rate $\dot{a}$ along the semi-major axis a for a binary and a disk that have the same configuration as in figure (2). At initially large values of the semi-major axis, the rate $\dot{a}_{\text{disk-binary}}$ dominates over $\dot{a}_{\text{GW}}$. In the purely disk-driven regime we find from equations (10) and (13) that the semi-major axis evolves as

$$\dot{a}_{\text{disk-binary}} \propto -a^{5/2} \left(1 + a^{-1/4}\right)^2 . \tag{15}$$

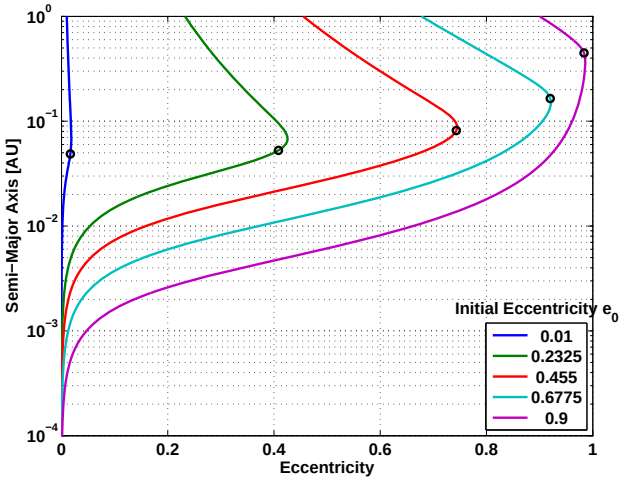

Fig. 2. The orbital semi-major axis as a function of the orbit's eccentricity for a binary systems premised on the evolution equations (14). In this plot we show $a(e)$ for different initial eccentricities. The disk-binary interaction decreases the orbit's semi-major axis and increases the orbit's eccentricity. The last stages of the orbital evolution are driven by gravitational wave emission and this causes the merging of the binary. The black dots indicate where gravitational wave emission takes over the disk driven interaction.

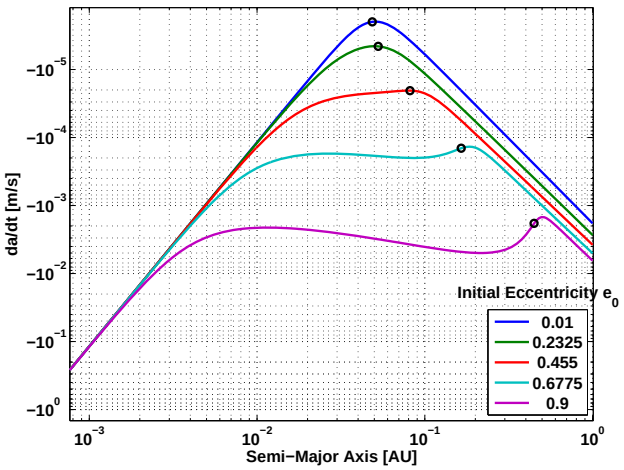

Fig. 3. The orbital decay rate is plotted as a function of the orbital separation of the binary for different initial eccentricities. At high values of a, the evolution of the semi-major axis is dictated by the disk-binary interaction, at small values of a by gravitational wave emission. The black dots indicate as in figure (2) the transition between the two regimes.

Only at sufficiently small semi-major axis the gravitational wave emission starts governing the orbital decay. The black circles in figure (3) show again the transition where $\dot{a}_{\rm GW}$ starts dominating over $\dot{a}_{\text{disk-binary}}$. The explicit expression for the dependence of the orbital decay rate on the semi-major axis in the gravitational wave driven regime is complicated, but can be extracted by inserting the inverse of equation (**??**) into (1). We see from figure (2) that when the semi-major axis has reached $a \sim 10^{-3} - 10^{-4}$ AU, the orbit has nearly circularized. Therefore during and after this regime the orbital evolution is purely gravitational wave driven and consequently the slope of the orbital decay is

$$\dot{a}_{\rm GW} \propto -a^{-3}. \tag{16}$$

With regards to the binary inspiral, in this binary evolution model the disk-interaction has two primary roles: The shrinking of the semi-major axis to a regime from which gravitational wave emission induces the merging and the orbital eccentricity pumping. Both effects contribute to a faster coalescence as compared to the purely gravitational wave evolution channel. Table (**??**) provides once more numerical examples. There we list $e_{\rm max}$, $a(e_{\rm max})$ and the merger time for binary systems where only a selected binary parameter is varied. The parameters which are not varied have the fiducial values: For the disk characteristics, $M_{\rm SMBH} = 1 \times 10^7 M_\odot, \alpha = 0.1, f_g = 0.1$ and $h/r = 0.01$, for the binary characteristics $r = 0.1$ pc and $a_0 = 1$ AU, $e_0 = 0.3$, $M = 50 M_\odot$ and $q = 1$. The maximal eccentricity $e_{\rm max}$ that is reached during the binary evolution increases as e_0 and a_0 increase and decreases as M and q increase. These dependencies reflect themselves also in the merger time dependence: The higher e_0 and a_0, the faster the coalescence and the higher M and q, the longer it takes the binary to merge. In contrast, for an orbital evolution purely driven by gravitational waves the merger time decreases as e_0, M and q increase and increases as a_0 increase. We observe from the a_0-entries the prominent effect of the eccentricity increase on the merger time: For low merger times, gravitational wave emission alone favours high eccentricities at the transition whereas smaller transition semi-major axis do not necessarily lead to lower merger times. The radial location r of the binary in the disk and the mass $M_{\rm SMBH}$ of the SMBH enter, of course, only $\dot{a}_{\text{disk-binary}}$ and $\dot{e}_{\text{disk-binary}}$. Because the dependence goes approximately as $M_{\rm SMBH}^{3/2}/r^2$, smaller r and higher $M_{\rm SMBH}$ enhance orbital shrinking and eccentricity pumping and foster therefore a faster coalescence.

4. Merger rate density estimates

In this section we want to investigate the binary black hole (BBH) merger rate density that could be expected from the binary evolution channel of the previous chapter. The merger rate density we take as the number of coalescences per unit time per unit volume.

In McKernan et al. (2018) the merger rate density of black hole binary mergers in AGN disks is parametrized as

$$\mathcal{R}_{\rm McK} = \frac{N_{\rm BHs}\, f_b\, f_d\, n_{\rm AGN}}{\tau_{\rm avg}}. \tag{17}$$

Here $N_{\rm BHs}$ is the number of stellar mass black holes per galactic nucleus, f_b is the fraction of black holes residing within binaries, f_d is the fraction of black holes embedded in the AGN disk (that is, $N_{\rm BHs} f_b f_d/2$ is the number of binary black holes embedded in the disk), $n_{\rm AGN}$ is the number density of active galactic nuclei and $\tau_{\rm avg}$ is the average binary merger time. In McKernan *et al.* the prescription (17) is taken as a starting point, however, no attempt is then made to estimate the average merger time of binary systems (it is instead assumed that all binaries merge within the lifetime of the disk). We will not resort to an average time scale when computing rates (because it underestimates BBH mergers with merger times smaller than $\tau_{\rm avg}$ and overestimates BBHs with merger times higher than $\tau_{\rm avg}$), but instead determine the merger rate density from a weighted average of the merger times of a population of BBHs.

4.1. Mass distributions

We will combine different mass distributions and mass density profiles to derive an expression for the number of black holes with a given mass range that reside within a radial shell of an AGN disk.

4.1.1. Stellar distribution

We start with an initial stellar population. The initial stellar mass distribution seems to follow a multiple power-law function. Here we adopt the initial stellar mass function of Kroupa (2002)

$$f_{\rm IMF}(m) = \begin{cases} k_0 \left(\frac{m}{M_\odot}\right)^{-0.3} & \text{if } m < 0.08 M_\odot \\ k_1 \left(\frac{m}{M_\odot}\right)^{-1.3} & \text{if } 0.08 M_\odot < m < 0.5 M_\odot \\ k_2 \left(\frac{m}{M_\odot}\right)^{-2.3} & \text{if } m > 0.5 M_\odot \end{cases}, \tag{18}$$

with the normalization parameters $k_0, k_1 = 0.08 k_0$ and $k_2 = 0.04 k_0$. We assume that the lowest mass of the stars $m_{\rm s,min}$ is smaller than $0.08 M_\odot$ and that the highest mass $m_{\rm s,max}$ is above $0.5 M_\odot$. The total number of stars is $N_* = \int_{m_{\rm s,min}}^{m_{\rm s,max}} dm f_{\rm IMF}(m)$ and the total stellar mass is $M_* = \int_{m_{\rm s,min}}^{m_{\rm s,max}} dm\, m f_{\rm IMF}$. For the stellar density profile $\rho_*(r)$, we adopt the "Nuker law" parametrization (Lauer et al. (1995))

$$\rho_*(r) \propto \left(\frac{r_b}{r}\right)^\gamma \left[1 + \left(\frac{r}{r_b}\right)^\alpha\right]^{\frac{\gamma-\beta}{\alpha}}, \tag{19}$$

and simplify it by using its asymptomatic slopes,

$$\rho_*(r) = \begin{cases} \rho_0 \left(\frac{r}{r_b}\right)^{-\gamma} & \text{if } r \le r_b \\ \rho_0 \left(\frac{r}{r_b}\right)^{-\beta} & \text{if } r > r_b \end{cases}. \tag{20}$$

The break radius r_b is approximately on the order of the radius of influence of the SMBH (Schödel, R. et al. (2018)), characterized as $r_b = M_{\rm SMBH}/\sigma^2$ (σ is the stellar dispersion).

4.1.2. BH distribution

If we assume that every star heavier than $m_{\rm s,cr} \sim 5 M_\odot$ evolved into a BH, the total number of BHs is

$$N_{\rm BHs} = \int_{m_{\rm s,cr}}^{m_{\rm s,max}} dm\, f_{\rm IMF} = k M_*, \tag{21}$$

where we defined

$$k = \frac{1}{M_\odot} \frac{-\frac{0.04}{1.3}\left[\left(\frac{m_{\rm s,max}}{M_\odot}\right)^{-1.3} - \left(\frac{m_{\rm s,cr}}{M_\odot}\right)^{-1.3}\right]}{\left[0.22 - \frac{1}{1.7}\left(\frac{m_{\rm s,min}}{M_\odot}\right)^{1.7} - \frac{0.04}{0.3}\left(\frac{m_{\rm s,max}}{M_\odot}\right)^{-0.3}\right]}. \tag{22}$$

The total mass of all BHs is

$$M_{\rm BH} = \int_{m_{\rm s,cr}}^{m_{\rm s,max}} dm\, m\, f_{\rm IMF}. \tag{23}$$

The BH mass distribution is denoted as $f_{\rm BH}(m)$ and is normalized such that $\int dm f_{\rm BH}(m) = 1$. We adopt a power-law mass function for the BH distribution

$$f_{\rm BH}(m) = \xi_0 m^{-\kappa}. \tag{24}$$

For $\kappa = 2.35$, we have a Salpeter mass function. If $N(r)$ denotes the total number of BHs inside some radius r, we take the number dN of BHs lying inside r with masses between m and $m + dm$ to be

$$dN = N(r) f_{\rm BH}(m) dm \tag{25}$$

$$= k M_*(r) f_{\rm BH}(m) dm, \tag{26}$$

where $M_*(r)$ is the total stellar mass inside radius r ($M_*(\infty) \equiv M_*$). Note that for the last equality we assumed that the mass distribution of the BHs is independent of the radius at which they reside. We can write dN in the following form

$$dN = dm\, k\, f_{\rm BH}(m) \int_0^r dr\, \rho_*(r) 4\pi r^2. \tag{27}$$

The number of BHs with masses between m and $m + dm$ in a radial shell from radius r to $r + dr$ is accordingly

$$\begin{cases} dm\, k\, f_{\rm BH}(m)\, \frac{4\pi\rho_0}{3-\gamma} r_b^\gamma \left[(r+dr)^{3-\gamma} - r^{3-\gamma}\right] & \text{if } r \le r_b \\ dm\, k\, f_{\rm BH}(m)\, \frac{4\pi\rho_0}{3-\beta} r_b^3 \left[\left(\frac{r+dr}{r_b}\right)^{3-\beta} - \left(\frac{r}{r_b}\right)^{3-\beta}\right] & \text{if } r > r_b \end{cases}. \tag{28}$$

4.2. Rate per galactic nucleus

To estimate the merger rate per galactic nucleus, we add up the rate contributions coming from different radial shells. We assume that the AGN disk around the supermassive black hole extends from $r_{\rm min}$ to $r_{\rm max}$. We partition the disk into $\mathcal{I}_r$ intervals. We denote by N_j the number of BHs within a radial shell $[r_{\rm min} + j\Delta r, r_{\rm min} + (j+1)\Delta r]$, where $\Delta r = (r_{\rm max} - r_{\rm min})/|\mathcal{I}_r|$. The mean radius of a radial shell is $r_j = r_{\rm min} + (j + 0.5)\Delta r$. The number of BBHs within each radial shell that are embedded in the disk is given by $N_{{\rm BBH},j} = N_j f_b f_d / 2$.

4.2.1. BBH distributions in a radial shell

Within each radial shell labelled by j we distribute the number of BBHs $N_{{\rm BBH},j}$ for the binary parameter $(m_1, m_2, e_0, a_0) \cong (m_1 \equiv \tilde{M}, q, e_0, a_0)$ according to some canonical binary parameter distribution functions. We assume for simplicity that the binary parameter distributions are independent from each other. The distributions in this subsection are normalized with respect to $N_{{\rm BBH},j}$.

Primary mass distribution We adopt the initial mass function (24) for the primary mass distribution. Thus, in a radial shell j the number of binaries with primary mass between m and $m + dm$ can be obtained from (28).

Secondary mass distribution The secondary mass distribution is determined by the distribution of the mass ratio q, assumed to follow a uniform distribution

$$f(q) = \vartheta_0, \tag{29}$$

where ϑ_0 is a constant and $q_{\rm min} \le q \le q_{\rm max}$.

Orbital separation distribution The distribution of the initial orbital separation a_0 is assumed to be logarithmically flat

$$f(a_0) = \chi_0 / a_0, \tag{30}$$

between the limits $a_{0,\rm min}$ and $a_{0,\rm max}$. This distribution is biased towards low semi-major axis.

Orbital eccentricity distribution We choose the distribution of the initial orbital eccentricity e_0 to follow a thermal distribution

$$f(e_0) = \varsigma_0 e_0, \tag{31}$$

between the limits $e_{0,\min}$ and $e_{0,\max}$. The number of BBHs below a given eccentricity e scale in a thermal distribution as e^2, a thermal distribution thus favours high eccentricities.

4.2.2. Calculation of rate within a radial shell

To calculate the rate of coalescences in a radial shell j, we partition each binary parameter into bins and distribute $N_{\mathrm{BBH},j}$ among the different bins. The merger rate is then determined as follows:

The quantities $\mathcal{I}_x$ (where x is one of $\tilde{M}, q, e_0$ or a_0) will denote the number of bins for the corresponding binary distributions x. We denote by $N_{x,i}$ the number of BBHs residing within the bin $i \in \mathcal{I}_x$ of the binary distribution x and denote by x_i the average of the variable x within bin i. We need to calculate for all possible combinations of $\lambda \in \mathcal{I}_{\tilde{M}} \times \mathcal{I}_q \times \mathcal{I}_{a_0} \times \mathcal{I}_{e_0}$ $\mathcal{I}_{\tilde{M}}$ the merger time $\tau_{\mathrm{merger},\lambda}$. We take as the input values needed for the numerical calculation of the merger time the average quantities x_i of the orbital parameter x in bin i. The total merger rate resulting from a radial shell j is therefore

$$\mathcal{R}_j = \sum_\lambda \frac{N_\lambda}{N^3_{\mathrm{BBH},j}} \frac{1}{\tau_{\mathrm{merger},\lambda}}, \tag{32}$$

where the sum goes over all $\lambda \in \mathcal{I}_{\tilde{M}} \times \mathcal{I}_q \times \mathcal{I}_{a_0} \times \mathcal{I}_{e_0}$ and where N_λ is the number of BBHs residing with the binning configuration λ.

We operated with the binning $\mathcal{I}_r = \mathcal{I}_{e_0} = 20$ and $\mathcal{I}_{\tilde{M}} = \mathcal{I}_q = \mathcal{I}_{a_0} = 10$, as it was both stable with respect to finer binnings and computationally economical.

4.2.3. Merger rate for a galactic nucleus

The merger rate for a galactic nucleus is obtained by summing up the rate (32) for each radial shell j

$$\mathcal{R}_{\mathrm{gal}} = \sum_{j \in \mathcal{I}_r} \mathcal{R}_j. \tag{33}$$

4.3. Merger rate density

The merger rate density $\mathcal{R}$ is given by

$$\mathcal{R} = \mathcal{R}_{\mathrm{gal}}\, n_{\mathrm{AGN}}. \tag{34}$$

The number N_* of stars within $r_{\max}$, the fraction f_b of BH in BBHs, the fraction f_d of BHs embedded in the disk and the number density n_{AGN} of active galactic nuclei affect the merger rate density $\mathcal{R}$ only as scaling factors and we report rate densities in a form where we have set these to a fixed value. For f_b, f_d and n_{AGN} we adopt the population parameters from McKernan et al. (2018) (in parenthesis we indicate the lower bound and upper bound)

- The fraction f_b of BH in BBH we estimate as 0.1 $[0.01, 0.2]$
- The fraction f_d of BH embedded in the disk we estimate as 0.01 $[0.01, 0.7]$
- The number density n_{AGN} of active galactic nuclei we estimate as 4×10^4 Gpc^{-3} $[4 \times 10^4$ Gpc^{-3}, 3×10^6 Gpc$^{-3}]$

In addition we fix $r_{\max} = 1$ pc. The inner edge of the accretion disk can in principle go down to about a few Schwarzschild radii, but we don't expect binaries to reside there. So we set fiducially $r_{\min}$ to 100 times the Schwarzschild radius of the SMBH. The number N_* of stars residing within 1 pc we estimate as 1×10^6. Furthermore, we use the fiducial values $m_{\mathrm{s},\min} = 0.01 M_\odot$, $m_{\mathrm{s},\max} = 200 M_\odot$ and $m_{\mathrm{s,cr}} = 5 M_\odot$. The number of BHs within 1 pc, obtained from formula (21), is then about 7.5×10^3, a value in accordance with the lower bound 10^3 and upper bound 10^6 adopted in McKernan *et al.*

Additionally we use all over the fiducial values $\beta = 3.2$ and $\gamma = 1.5$ for the mass distribution parameters. Also we adopt throughout a disk aspect ratio $h/r = 0.01$, a gas fraction $f_g = 0.1$ and a viscosity parameter $\alpha = 0.1$.

Unless not subject to variation, we use $M_{\mathrm{SMBH}} = 1 \times 10^7\, M_\odot$ and adopt a Salpeter mass function, *i.e.* we set $\kappa = 2.35$. Unless a binary parameter is not subject to variation, we use the respective distributions of section (4.2.1) and the following ranges of the orbital parameters

- $[m_{\mathrm{BH},\min}, m_{\mathrm{BH},\max}] = [5, 50]\, M_\odot$,
- $[q_{\min}, q_{\max}] = [0.1, 1]$,
- $[a_{0,\min}, a_{0,\max}] = [1, 100]$ AU,
- $[e_{0,\min}, e_{0,\max}] = [0.001, 0.99]$.

In tables (XX) to (XX) we document the average and median merger time and the merger rate density for various choices of the orbit and disk configurations. In each table one parameter is subject to variation. For comparison, each table also includes the result of the canonical parameter configuration. For the canonical orbital distributions, the merger rate densities vary between 0.05 year^{-1} Gpc^{-3} and 3 year^{-1} Gpc^{-3}. For comparison, the purely gravitational wave driven merger rate density for the canonical parameter choices is as low as 8×10^{-11} year^{-1} Gpc^{-3}. The change in each rate density within a selected parameter regime follows the expected trend of section (**??**), see especially table (**??**). We want to highlight the importance of eccentric orbits on the merger rate density: A population of nearly circular binaries yields a rate density of about 6×10^{-6} year^{-1} Gpc^{-3}, whereas distributions across all eccentricities give rate densities of about 5 orders of magnitude higher. The median and average merger time differ generally by about two orders of magnitudes, which attests once more the inadequacy of resorting to average merger time scales for rate estimates.

The current LIGO and Virgo stellar mass binary black hole merger rate density is $24 - 112$ year^{-1} Gpc^{-3} (The LIGO Scientific Collaboration et al. (2018)). A notable part of the gravitational wave detections could thus originate from binaries undergoing the AGN evolution channel outlined here. The here reported rate densities are nevertheless considerably lower than the rate densities expected to be monitored by future gravitational wave detectors. We list two reasons for this deviation. First of all, only a subset of the mergers detectable by LIGO actually originate from active galactic nuclei. Secondly, many variables ($N_*, f_b, n_{\mathrm{AGN}}$, etc.) that went into the rate density calculation display large uncertainties. Our fiducial choices for those variables lie on the lower spectrum of the uncertainty ranges. And it has to be emphasized once more that the here detailed rate densities are based on many assumptions, in particular a very simplified and idealised model of the disk-binary interaction. That being said, one can conclude on good grounds that disk interactions, whatever they be, likely have a prominent

influence on the merger rate density. As already pointed out, neglecting mechanisms in the orbital binary evolution apart from gravitational wave emission stands in strong discrepancy to the current LIGO merger rate density estimates.

$M_{\rm SMBH}$	old $1\times10^6\,M_\odot$	$1\times10^7\,M_\odot$	old $1\times10^8\,M_\odot$
$\tau_{\rm avg}$ [years]	3.12×10^9	2.41×10^8	1.75×10^7
$\tau_{\rm med}$ [years]	1.59×10^8	6.96×10^6	2.58×10^5
$\mathcal{R}$ [year^{-1} Gpc^{-3}]	3.9×10^{-2}	0.18	0.72

Initial eccentricity	Thermal distribution between [0.001, 0.99]	Uniform distribution between [0.001, 0.99]	Delta distribution at $e_0 = 0.001$
$\tau_{\rm avg}$ [years]	1.75×10^7	1.80×10^7	1.49×10^8
$\tau_{\rm med}$ [years]	2.58×10^5	2.60×10^5	1.23×10^8
$\mathcal{R}$ [year^{-1} Gpc^{-3}]	0.72	0.40	5.68×10^{-6}

κ	1.35	2.35	2.85
$\tau_{\rm avg}$ [years]	1.75×10^7	1.75×10^7	1.75×10^7
$\tau_{\rm med}$ [years]	2.60×10^5	2.58×10^5	2.57×10^5
$\mathcal{R}$ [year^{-1} Gpc^{-3}]	0.49	0.72	0.82

Mass ratio	Uniform distribution between [0.01, 1]	Uniform distribution between [0.1, 1]	Delta distribution at $q = 1$
$\tau_{\rm avg}$ [years]	1.75×10^7	1.85×10^7	2.31×10^7
$\tau_{\rm med}$ [years]	2.58×10^5	3.02×10^5	5.25×10^5
$\mathcal{R}$ [year^{-1} Gpc^{-3}]	0.72	0.50	0.24

Initial semi-major axis	Log-flat distribution between [0.1, 100] AU	Uniform distribution between [0.1, 100] AU
$\tau_{\rm avg}$ [years]	1.75×10^7	1.68×10^7
$\tau_{\rm med}$ [years]	2.58×10^5	2.26×10^5
$\mathcal{R}$ [year^{-1} Gpc^{-3}]	0.72	3.03

Orbital evolution	Gravitational wave driven	Gravitational wave and disk driven
$\tau_{\rm avg}$ [years]	3.88×10^{21}	1.75×10^7
$\tau_{\rm med}$ [years]	2.52×10^{19}	2.58×10^5
$\mathcal{R}$ [year^{-1} Gpc^{-3}]	8.38×10^{-11}	0.72

5. Discussion

References

Artymowicz, P. & Lubow, S. H. 1994, The Astrophysical Journal, 421, 651

Baruteau, C., Cuadra, J., & Lin, D. N. C. 2010, The Astrophysical Journal, 726, 28

Hayasaki, K., Mineshige, S., & Sudou, H. 2007, Publications of the Astronomical Society of Japan, 59, 427

Kroupa, P. 2002, Science, 295, 82

Lauer, T. R., Ajhar, E. A., Byun, Y.-I., et al. 1995, The Astrophysical Journal, 110, 2622

Lubow, S. H. & Artymowicz, P. 1996, Evolutionary Processes in Binary Stars, ed. . C. A. T. R. A. M. J. Wijers, M. B. Davies (NATO ASIC Proc. 477)

McKernan, B., Ford, K. E. S., Bellovary, J., et al. 2018, The Astrophysical Journal, 866, 66

Peters, P. C. & Mathews, J. 1963, Phys. Rev., 131, 435

Schödel, R., Gallego-Cano, E., Dong, H., et al. 2018, A&A, 609, A27

The LIGO Scientific Collaboration, the Virgo Collaboration, Abbott, B. P., et al. 2018, arXiv e-prints [arXiv:1811.12940]